Multilayered $PdTe_2$/GaN Heterostructures for Visible-Blind Deep-Ultraviolet Photodetection

Yi Liang, Mengru Ma, Xianpeng Zhong, Chao Xie, Xiaowei Tong, Kun Xing, and Chunyan Wu

***Abstract*— Deep-ultraviolet (DUV) photodetection has garnered extensive research interest for its vital applications in many military and civil fields. In this work, we present the synthesis of a large-area two-dimensional (2D) $PdTe_2$ multilayer, which can be directly transferred onto a GaN substrate to construct a vertical heterostructure for visible-blind DUV photodetection. Upon 265 nm light irradiation, the heterostructure displays a distinct photovoltaic behavior, enabling it to serve as a self-driven photodetector. The important photoresponse parameters, such as I_{light}/I_{dark} ratio, responsivity, specific detectivity and DUV/visible (265 nm/450 nm) rejection ratio reach as high as 10^6, 168.5 mA/W, 5.3 × 10^{12} Jones, and 10^4, respectively, at zero bias. The responsivity can be further enhanced to 254.6 mA/W by applying a small reverse bias of −1.0 V. In addition, the photodetector can function as a DUV light image sensor to reliably record an "H" pattern with a decent resolution. The present study paves a way for designing high-performance cost-effective DUV photodetectors towards practical optoelectronic applications.**

***Index Terms*— Deep-ultraviolet, visible-blind, heterostructure, photodetector, image sensor.**

I. Introduction

LIGHT detection in the deep-ultraviolet (DUV, typically 190-350 nm) spectrum region has long attracted enormous attention due to its significant applications in military and civil areas [1]. Traditionally, DUV photodetection is dominated by photomultiplier tubes (PMTs) and ultraviolet (UV)-enhanced Si photodiodes [2]. However, PMTs require high working voltages and are also heavy and bulky, while Si photodiodes have challenges of filter dependence, limited quantum efficiency and low DUV/visible rejection ratio [3]. Comparatively, wide-bandgap semiconductors (e.g., GaN and SiC) and ultrawide-bandgap semiconductors (e.g., Ga_2O_3, $Al_xGa_{1-x}N$ and $Mg_xZn_{1-x}O$) holding advantages of large bandgaps, high thermal conductivities and high electron velocities at large electric fields, are extremely suitable for DUV photodetection [4]. To date, a series of DUV photodetectors (PDs) have been developed with these materials [2]. Among them, the study of photodiodes is of particular interest owing to the features of attaining high-speed response, low dark current and noise, high specific detectivity (D^*), *etc*. Nevertheless, their development and application are greatly hindered by difficulties such as strictly required epitaxial growth conditions, realization of effective doping and ohmic contacts [5]. Combining these semiconductors with other materials to form heterostructures offer an alternative solution for circumventing the dilemma.

In recent years, two-dimensional (2D) materials have been extensively explored for developing PDs due to their versatile and prominent characteristics [6], [7]. In particular, their weak van der Waals interactions between adjacent layers allows the assembly of various heterostructures beyond the limitation of lattice matching towards high-performance photodetection. As a novel group-10 transition metal dichalcogenide, $PdTe_2$ exhibits features of topological superconductivity and type-II Dirac fermions, combined with high carrier mobility and excellent ambient stability, and has therefore garnered huge attention to condensed matter physics [8], [9]. Nevertheless, large-area preparation of 2D $PdTe_2$ and its application in optoelectronic areas are rarely reported by far.

Here, we report synthesis of large-area 2D $PdTe_2$ multilayers through directly tellurization of Pd ultrathin films. The combination of $PdTe_2$ with GaN results in the formation of a heterostructure, which serves well as a visible-blind DUV PD with eminent photoresponse performance. The functionality to operate as a DUV light image senor is also demonstrated.

II. Experiments

The $PdTe_2$ multilayer was synthesized by tellurizing a Pd ultrathin film. A ~6 nm Pd film was firstly deposited onto a cleaned SiO_2 (300 nm)/Si substrate *via* electron beam evaporation. Then, the substrate was transferred to the central zone of a tube furnace, and a boat containing 0.5 g Te powder was placed upstream. The furnace was heated to 300 °C and kept for 1 h to allow tellurization, during which a 100 sccm Ar gas was employed to carry the evaporated gas towards downstream. The as-synthesized $PdTe_2$ was characterized by scanning electron microscope (SEM), Raman, X-ray diffraction (XRD) and atomic force microscope (AFM), respectively.

Manuscript received May 18, 2021; revised June 2, 2021; accepted June 5, 2021. Date of publication June 9, 2021; date of current version July 26, 2021. This work was supported in part by the National Natural Science Foundation of China (NSFC) under Grant 51902078, in part by the Anhui Provincial Natural Science Foundation under Grant 2008085MF205, and in part by the Fundamental Research Funds for the Central Universities under Grant JZ2020HGTB0051. The review of this letter was arranged by Editor L. K. Nanver. *(Corresponding authors: Chao Xie; Kun Xing; Chunyan Wu.)*

Yi Liang, Mengru Ma, Xianpeng Zhong, Xiaowei Tong, Kun Xing, and Chunyan Wu are with the School of Microelectronics, Hefei University of Technology, Hefei 230009, China (e-mail: k.xing@hfut.edu.cn; cywu@hfut.edu.cn).

Chao Xie is with the School of Microelectronics, Hefei University of Technology, Hefei 230009, China, and also with the School of Electronics and Information Engineering, Anhui University, Hefei 230601, China (e-mail: chaoxie@ahu.edu.cn).

Color versions of one or more figures in this letter are available at https://doi.org/10.1109/LED.2021.3087704.

Digital Object Identifier 10.1109/LED.2021.3087704

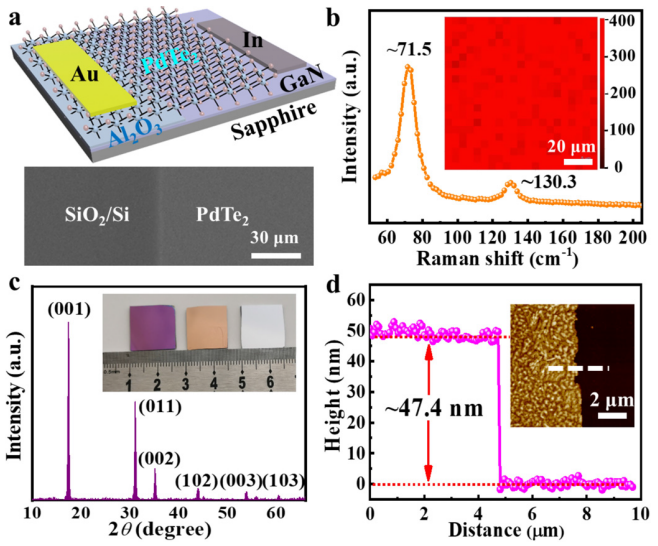

Fig. 1. (a) Top panel: schematic diagram of the $PdTe_2$/GaN heterostructure PD. Bottom panel: SEM image of the $PdTe_2$ multilayer. (b) Raman spectrum, (c) XRD pattern and (d) height profile of the $PdTe_2$ multilayer. Inset in (b), (c) and (d) shows the 2D Raman mapping, optical image (left, middle and right are SiO_2/Si, SiO_2/Si covered with Pd film, and SiO_2/Si covered with $PdTe_2$ layer, respectively), and AFM image.

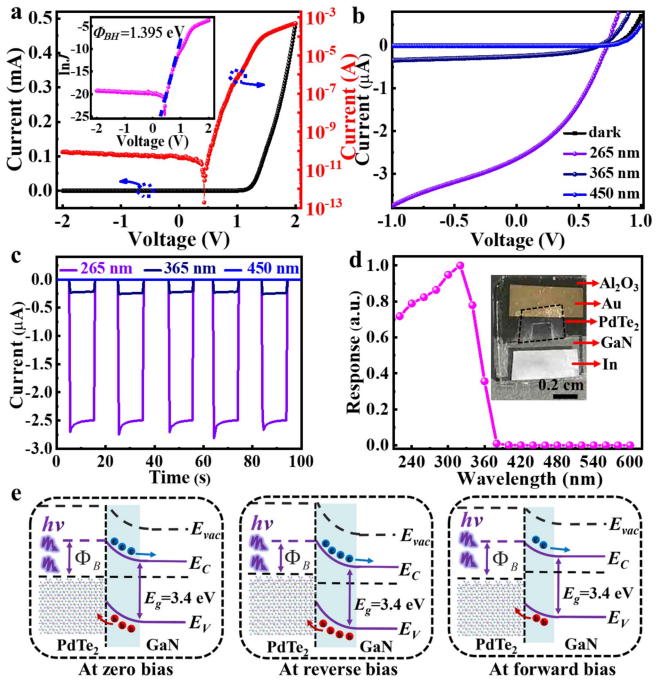

Fig. 2. *I–V* curves (a) at both linear and semi-logarithmic scales in dark, (b) in dark and under 265, 365 and 450 nm illuminations. Inset in (a) shows the ln *J–V* curve for calculating the barrier height. (c) Time-dependent photoresponse under 265, 365 and 450 nm illuminations. (d) Photoresponse as a function of light wavelength. Inset in (d) shows an optical image of the $PdTe_2$/GaN heterostructure PD. (e) Energy band diagrams of the heterostructure at different working biases.

The PD was fabricated by transferring a $PdTe_2$ multilayer onto a GaN epitaxial layer covered partially with ~80 nm AlO_x insulting layer *via* a PMMA-assisted transfer technique [10]. The used GaN epitaxial layer (~6 μm in thickness, Si-doped, resistivity: ~0.016 Ω·cm) was grown on an intrinsic GaN layer/sapphire (650 μm) substrate through a metal organic chemical vapor deposition process. 100 nm Au and 200 nm In were evaporated onto $PdTe_2$ and GaN to serve as ohmic contacts, respectively (Fig. 1a, top panel). Electrical measurements were conducted on a Keithley 4200-SCS semiconductor analyzer, and 265, 365, 450 and 530 nm laser diodes were used as light sources.

III. Results and Discussion

SEM image of $PdTe_2$ multilayer shows a large-area film with a smooth surface (Fig. 1a, bottom panel). Raman spectrum depicts two prominent peaks located at about 71.5 cm^{-1} and 130.3 cm^{-1}, which could be assigned to the in-plane (E_g) and out-of-plane (A_{1g}) motions of Te atoms, respectively (Fig. 1b) [11]. 2D Raman mapping conducted on $PdTe_2$ multilayer transferred atop GaN shows very narrow peak intensity distribution of A_{1g} active mode (inset in Fig. 1b), implying a high continuity and homogeneity of the sample. XRD pattern displays six diffraction peaks positioned at 17.28°, 30.94°, 34.96°, 43.96°, 53.55° and 60.46°, corresponding to (001), (011), (002), (102), (003) and (103) crystal planes of $PdTe_2$ (JCPDS Card No. 88-2279), respectively (Fig. 1c). This result together with AFM image (inset in Fig. 1d) indicates that the as-synthesized $PdTe_2$ was a polycrystalline film consisting of sub-micrometer sized crystalline domains. The thickness was determined to be ~47.4 nm.

Fig. 2a plots the current-voltage (I–V) curve of the heterostructure, signifying a typical rectifying behavior with the rectification ratio of ~5.65×10^6 within ±2 V. The barrier height and ideality factor were calculated to be ~1.34 eV (inset in Fig. 2a) and ~1.03, respectively, confirming the high-quality of the heterojunction. Fig. 2b compares the I–V curves in dark and under illuminations with different wavelengths (at a fixed light intensity: ~1 $mWcm^{-2}$). Significantly, the heterostructure displayed a remarkable response to 265 nm illumination, about 10 times higher than that to 365 nm illumination, and was nearly in-sensitive to 450 nm illumination. In particular, a pronounced photovoltaic (PV) effect with an open-circuit voltage of 0.725 V and a short-circuit current of 2.52 μA was observed under 265 nm irradiation, enabling the heterostructure to operate as a self-driven PD. Fig. 2c depicts the transient photoresponse at zero bias, where the photocurrent showed the same evolution with the change of light wavelength as the I–V curves. The current rose remarkably from ~2.0 pA in dark to ~2.5 μA under 265 nm illumination and to ~0.24 μA under 365 nm illumination, rendering a large I_{light}/I_{dark} ratio exceeding 10^6 and 10^5, respectively. The sharp rise and fall edges implied rapid separation and collection of photoexcited carriers, and a fast response speed as well. Fig. 2d shows the photoresponse as a function of incident light wavelength. Apparently, the device exhibited a prominent photoresponse characteristic at DUV spectral region (220-360 nm) with a peak response at ~320 nm and a response cutoff at ~370 nm, signifying the visible-blind photodetection ability. The DUV/visible (265 nm/450 nm) rejection ratio exceeded 10^4.

The above photoresponse behavior could be understood from the energy band diagram. A built-in electric field with the direction from GaN to $PdTe_2$ was created at the heterostructure

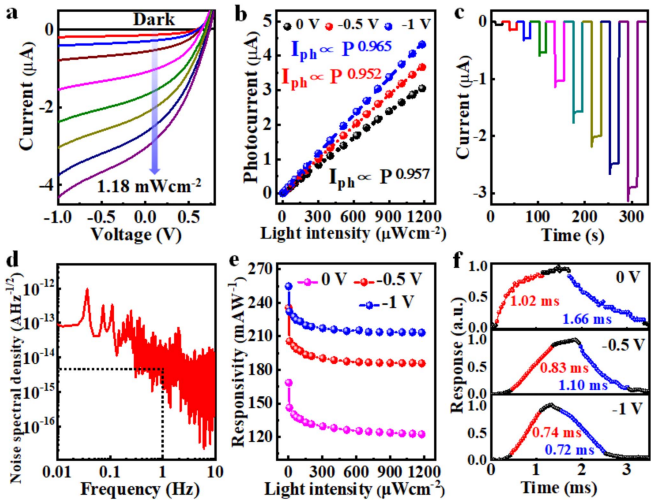

Fig. 3. (a) *I–V* curves and (c) transient photoresponse under 265 nm illumination with different intensities. (b) The photocurrent under varied biases as a function of light intensity. (d) Analysis of noise spectral density. (e) *R* under varied biases as a function of light intensity. (f) Magnified photoresponse curves at 280 Hz under different bias voltages for calculating response times.

interface when the metallic $PdTe_2$ with Fermi level of ∼4.8 eV (data not shown) was contact with n-GaN. When shinned by illumination with photon energy exceeding the bandgap of GaN, electron-hole pairs were excited within or near the depletion region. The carriers were then separated by the built-in electric field and propelled towards opposite directions, producing photocurrent at zero bias (Fig. 2e, left panel). Under reverse bias, an external electric field in the same direction with the built-in one facilitated the separation and transport of photocarriers, and extended the depletion region, rendering more photocarriers to participate in the generation of photocurrent (Fig. 2e, middle panel) [12]. On the contrary, a forward bias provided an external electric field opposite to the built-in one, which would retard the separation and transport of photocarriers, and shrunk the depletion region (Fig. 2e, right panel). Therefore, it was expected that the device would exhibit a superior photoresponse under reverse working bias.

Fig. 3a plots the *I–V* curves under 265 nm illumination with different intensities from 0.017 $mWcm^{-2}$ to 1.18 $mWcm^{-2}$. Apparently, the photocurrent at both zero and reverse biases increased gradually with increasing light intensity, which was attributed to the increased concentration of photocarriers at a higher light intensity. Fitting the curve of photocurrent *versus* light intensity at different biases with the relationship $I_{ph} \propto P^{\theta}$ gave all θ values closing to the ideal value of 1, signifying ignorable recombination loss at these working biases (Fig. 3b) [13]. In addition, transient photoresponse in Fig. 3c implied a reliable photo-switching characteristic for all illuminating conditions. Furthermore, the responsivity (R) and D^* were calculated following the equations: $R = \frac{I_{light} - I_{dark}}{SP}$, $D^* = \frac{(SB)^{1/2}}{NEP}$ and $NEP = \frac{\bar{i}_n^{21/2}}{R}$, where S, P, B, NEP and $\bar{i}_n^{21/2}$ are the effective device area (∼0.02 cm^2), light intensity, bandwidth, noise equivalent power and root-mean-square value of the noise current,

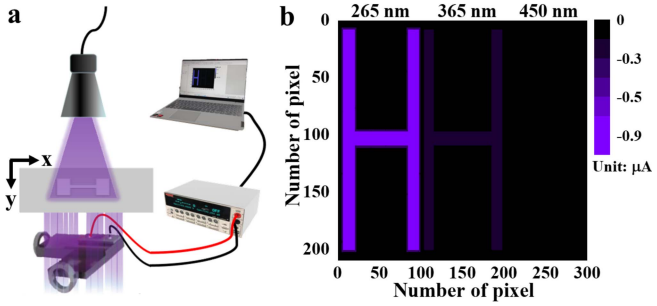

Fig. 4. (a) Schematic illustration of the setup for optical image sensing. (b) The 2D current contrast map under 265, 365 and 450 nm illuminations.

respectively [14]. The $\bar{i}_n^{21/2}$ was ∼4.5 $fAHz^{-1/2}$ at 1 Hz (Fig. 3d), giving a *NEP* of 2.7×10^{-14} $WHz^{-1/2}$. Therefore, the R and D^* were estimated to be ∼168.5 mAW^{-1} and 5.3×10^{12} Jones, respectively, at zero bias (light intensity: 1.53 μWcm^{-2}).

Fig. 3e shows the dependence of R on the light intensity at varied biases, indicating a slight decrease of R over a wide light intensity region. Specially, the value declined from ∼168.5 mAW^{-1} to ∼122.4 mAW^{-1} when the light intensity changed from 1.53 μWcm^{-2} to 1.18 $mWcm^{-2}$. Additionally, the R could be further improved by increasing reverse working bias, and the value increased from ∼168.5 mAW^{-1} to ∼235.4/∼254.6 mAW^{-1} at 1.53 μWcm^{-2} when the working bias changed from 0 V to -0.5/-1.0 V. Notably, the R value was comparable to that of previously reported GaN-based heterostructure DUV PDs [15]–[17]. Further, as observed in Fig. 3f, the rise/fall times were calculated to be 1.02/1.66 ms, 0.83/1.10 ms and 0.74/0.72 ms, at the working bias of 0 V, −0.5 V and −1.0 V. respectively. The enhanced responsivity and improved response speed at reverse working bias were consistent with the analysis in the energy band diagrams.

Finally, we explored the capability of our PD for optical image sensing. Light irradiation penetrating a hollow "H" pattern (size: 2.1 × 1.4 cm^2) was projected onto the PD, atop which a lab-made shadow mask with 100 × 100 μm^2 hollow square pattern was placed to define effective sensing area. A stepper motor was employed to drive the PD move along both x- and y-axes to collect the current in each pixel (Fig. 4a). All the current values corresponding pixels were summarized by a 2D contrast map. Fig. 4b plots the current map profiles under illumination of 265 nm, 365 nm and 450 nm. Obviously, the image under 265 nm illumination could be clearly identified with a much higher contrast than that under 365 nm illumination, while it was completely indistinguishable under 450 nm illumination. The results implied a great potential of the present PD for DUV light image sensing application.

IV. Conclusion

In summary, we have demonstrated a high-performance visible-blind DUV photodetector based on a heterostructure comprising a large-area 2D $PdTe_2$ multilayer transferred directly onto a GaN substrate. The prominent PV effect endowed the heterostructure with self-driven DUV photodetection capability, which could serve as a reliable DUV light image senor as well.

REFERENCES

[1] H. Chen, K. Liu, L. Hu, A. A. Al-Ghamdi, and X. Fang, "New concept ultraviolet photodetectors," *Mater. Today*, vol. 18, no. 9, pp. 493–502, Nov. 2015, doi: 10.1016/j.mattod.2015.06.001.

[2] C. Xie, X.-T. Lu, X.-W. Tong, Z.-X. Zhang, F.-X. Liang, L. Liang, L.-B. Luo, and Y.-C. Wu, "Recent progress in solar-blind deep-ultraviolet photodetectors based on inorganic ultrawide bandgap semiconductors," *Adv. Funct. Mater.*, vol. 29, no. 9, Feb. 2019, Art. no. 1806006, doi: 10.1002/adfm.201806006.

[3] M. Razeghi, "Short-wavelength solar-blind detectors-status, prospects, and markets," *Proc. IEEE*, vol. 90, no. 6, pp. 1006–1014, Jun. 2002, doi: 10.1109/jproc.2002.1021565.

[4] L. Sang, M. Liao, and M. Sumiya, "A comprehensive review of semiconductor ultraviolet photodetectors: From thin film to one-dimensional nanostructures," *Sensors*, vol. 13, no. 8, pp. 10482–10518, Aug. 2013, doi: 10.3390/s130810482.

[5] E. Monroy, F. S. Omn, and F. Calle, "Wide-bandgap semiconductor ultraviolet photodetectors," *Semicond. Sci. Technol.*, vol. 18, no. 4, pp. R33–R51, Apr. 2003, doi: 10.1088/0268-1242/18/4/201.

[6] F. H. L. Koppens, T. Mueller, P. Avouris, A. C. Ferrari, M. S. Vitiello, and M. Polini, "Photodetectors based on graphene, other two-dimensional materials and hybrid systems," *Nature Nanotechnol.*, vol. 9, no. 10, pp. 780–793, Oct. 2014, doi: 10.1038/nnano.2014.215.

[7] M. Buscema, J. O. Island, D. J. Groenendijk, S. I. Blanter, G. A. Steele, H. S. J. van der Zant, and A. Castellanos-Gomez, "Photocurrent generation with two-dimensional van der Waals semiconductors," *Chem. Soc. Rev.*, vol. 44, no. 11, pp. 3691–3718, 2015, doi: 10.1039/c5cs00106d.

[8] H.-J. Noh, J. Jeong, E.-J. Cho, K. Kim, B. I. Min, and B.-G. Park, "Experimental realization of type-II dirac fermions in a $PdTe_2$ superconductor," *Phys. Rev. Lett.*, vol. 119, no. 1, Jul. 2017, Art. no. 016401, doi: 10.1103/PhysRevLett.119.016401.

[9] L. Pi, L. Li, K. Liu, Q. Zhang, H. Li, and T. Zhai, "Recent progress on 2D noble-transition-metal dichalcogenides," *Adv. Funct. Mater.*, vol. 29, no. 51, Dec. 2019, Art. no. 1904932, doi: 10.1002/adfm.201904932.

[10] L.-H. Zeng, S.-H. Lin, Z.-J. Li, Z.-X. Zhang, T.-F. Zhang, C. Xie, C.-H. Mak, Y. Chai, S. P. Lau, L.-B. Luo, and Y. H. Tsang, "Fast, self-driven, air-stable, and broadband photodetector based on vertically aligned $PtSe_2$/GaAs heterojunction," *Adv. Funct. Mater.*, vol. 28, no. 16, Apr. 2018, Art. no. 1705970, doi: 10.1002/adfm.201705970.

[11] C. Guo, Y. Hu, G. Chen, D. Wei, L. Zhang, Z. Chen, W. Guo, H. Xu, C.-N. Kuo, C. S. Lue, X. Bo, X. Wan, L. Wang, A. Politano, X. Chen, and W. Lu, "Anisotropic ultrasensitive $PdTe_2$-based phototransistor for room-temperature long-wavelength detection," *Sci. Adv.*, vol. 6, no. 36, Sep. 2020, Art. no. eabb6500, doi: 10.1126/sciadv.abb6500.

[12] S. M. Sze and K. K. Ng, *Physics of Semiconductor Devices*. Hoboken, NJ, USA: Wiley, 2007, pp. 671–674.

[13] X. Li, M. Zhu, M. Du, Z. Lv, L. Zhang, Y. Li, Y. Yang, T. Yang, X. Li, K. Wang, H. Zhu, and Y. Fang, "High detectivity graphene-silicon heterojunction photodetector," *Small*, vol. 12, no. 5, pp. 595–601, Feb. 2016, doi: 10.1002/smll.201502336.

[14] C. Xie, Y. Wang, Z.-X. Zhang, D. Wang, and L.-B. Luo, "Graphene/semiconductor hybrid heterostructures for optoelectronic device applications," *Nano Today*, vol. 19, pp. 41–83, Apr. 2018, doi: 10.1016/j.nantod.2018.02.009.

[15] R. Zhuo, Y. Wang, D. Wu, Z. Lou, Z. Shi, T. Xu, J. Xu, Y. Tian, and X. Li, "High-performance self-powered deep ultraviolet photodetector based on MoS_2/GaN p–n heterojunction," *J. Mater. Chem. C*, vol. 6, no. 2, pp. 299–303, 2018, doi: 10.1039/C7TC04754A.

[16] Y. Zhu, K. Liu, Q. Ai, Q. Hou, X. Chen, Z. Zhang, X. Xie, B. Li, and D. Shen, "A high performance self-powered ultraviolet photodetector based on a p-GaN/n-ZnMgO heterojunction," *J. Mater. Chem. C*, vol. 8, no. 8, pp. 2719–2724, Feb. 2020, doi: 10.1039/C9TC06416H.

[17] R. Zhuo, L. Zeng, H. Yuan, D. Wu, Y. Wang, Z. Shi, T. Xu, Y. Tian, X. Li, and Y. H. Tsang, "*In-situ* fabrication of $PtSe_2$/GaN heterojunction for self-powered deep ultraviolet photodetector with ultrahigh current on/off ratio and detectivity," *Nano Res.*, vol. 12, no. 1, pp. 183–189, Jan. 2019, doi: 10.1007/s12274-018-2200-z.